2D Materials

PAPER • OPEN ACCESS

Direct growth of graphene on GaN via plasma-enhanced chemical vapor deposition under N_2 atmosphere

To cite this article: Jan Mischke *et al* 2020 *2D Mater.* **7** 035019

View the article online for updates and enhancements.

IOP Publishing 2D Mater. 7 (2020) 035019 https://doi.org/10.1088/2053-1583/ab8969

2D Materials

PAPER

OPEN ACCESS

RECEIVED
12 February 2020

REVISED
25 March 2020

ACCEPTED FOR PUBLICATION
15 April 2020

PUBLISHED
29 May 2020

Original content from this work may be used under the terms of the Creative Commons Attribution 4.0 licence.

Any further distribution of this work must maintain attribution to the author(s) and the title of the work, journal citation and DOI.

Direct growth of graphene on GaN via plasma-enhanced chemical vapor deposition under N_2 atmosphere

Jan Mischke[1], Joel Pennings[1,2], Erik Weisenseel[1], Philipp Kerger[3], Michael Rohwerder[3], Wolfgang Mertin[1] and Gerd Bacher[1]

[1] Werkstoffe der Elektrotechnik and CENIDE, Universität Duisburg-Essen, 47057 Duisburg, Germany
[2] Faculty of Engineering, University of Waterloo, Waterloo ON N2L 3G1 Canada
[3] Max-Planck-Institut für Eisenforschung GmbH, 40237 Düsseldorf, Germany

E-mail: gerd.bacher@uni-due.de

Keywords: PECVD, graphene, N_2 atmosphere, GaN, LED

Supplementary material for this article is available online

Abstract

One of the bottlenecks in the implementation of graphene as a transparent electrode in modern opto-electronic devices is the need for complicated and damaging transfer processes of high-quality graphene sheets onto the desired target substrates. Here, we study the direct, plasma-enhanced chemical vapor deposition (PECVD) growth of graphene on GaN-based light-emitting diodes (LEDs). By replacing the commonly used hydrogen (H_2) process gas with nitrogen (N_2), we were able to suppress GaN surface decomposition while simultaneously enabling graphene deposition at <800 °C in a single-step growth process. Optimizing the methane (CH_4) flow and varying the growth time between 0.5 h and 8 h, the electro-optical properties of the graphene layers could be tuned to sheet resistances as low as ∼1 kΩ/□ with a maximum transparency loss of ∼12%. The resulting high-quality graphene electrodes show an enhanced current spreading effect and an increase of the emission area by a factor of ∼8 in operating LEDs.

1. Introduction

The most common method to fabricate large scale, high-quality graphene sheets is chemical vapor deposition (CVD) due to its potential in scalability for graphene based applications [1]. Initial experiments to grow graphene via CVD mostly used high-temperature growth processes on catalytic substrates, like copper [2, 3] or nickel (Ni) [4, 5]. Down to the present day, researchers were able to increase quality and scalability to single crystalline, large-area graphene layers [6]. However, the growth of graphene on catalytic substrates is mostly followed by inevitable processes to transfer the graphene onto desired target substrates. These transfer processes can be very damaging to the graphene layers by inducing mechanical defects, contamination with residues of the used transfer solvents and doping effects [7]. To avoid these adverse transfer processes, direct growth of graphene onto the desired target substrate, e.g. by plasma-enhanced CVD (PECVD), was introduced. Here, the plasma is used for the dissociation process of the carbon containing precursor. Using this approach, more industrially relevant substrates like quartz [8, 9], sapphire [8, 9], mica [8, 10], SiO_2 [11, 12], germanium [13] and gallium nitride (GaN) [14–16] have been used for the direct growth of graphene.

GaN is widely established for the use in blue and white light-emitting diodes (LEDs) and is a highly promising material for modern ultraviolet (UV) LEDs [17] due to its tunable band gap by adding aluminum nitride, forming aluminum gallium nitride ($Al_xGa_{1-x}N$). By this band gap tuning, emission wavelengths of $Al_xGa_{1-x}N$-based LEDs can reach down to the deep UV-C spectrum (<280 nm). However, there are still some obstacles to overcome for UV-LEDs in order to become more efficient and to meet industrial expectations. One major problem is the low conductivity of the *p*-doped top layers, in particular with higher Al concentrations [17]. This problem makes the use of current spreading layers (CSL) inevitable. The commonly used indium tin oxide (ITO), which is a standard material for such CSLs in blue LEDs, cannot be used for UV-LEDs due to high optical absorption losses in the UV-B

and UV-C spectral range [18, 19]. Graphene, however, offers high optical transparencies of over 90% even down in the deep UV-C spectral range [18]. Combined with its outstanding electrical conductivity [20], graphene is a promising material for transparent CSLs in novel UV-LEDs.

Jo *et al* were the first to successfully prove the possibility of using transferred, multilayer CVD graphene as a current spreading layer on fully-processed, blue GaN LEDs [21], with transparencies of ~85%. However, due to the transfer process of the graphene onto the GaN-based LED, the contact resistance between the graphene and the top *p*-GaN layer was drastically increased when compared to state-of-the-art ITO CSLs. Consequently, different interlayers like Ag nanowires [22, 23], ITO [24], Ni/Au [25, 26] and NiO_x [27–29] have been introduced to improve the contact resistance between the transferred graphene and the top *p*-GaN layer. However, the lower contact resistances associated with these interlayers came with a trade-off in higher absorption losses.

To overcome these problems, few groups have investigated the transfer free, direct growth of graphene on GaN-based substrates. Sun *et al* were the first to attempt the direct growth of graphene on GaN via thermal CVD at 950 °C [30]. The grown layers showed very high sheet resistances and large amounts of sp^3-hybridized carbon. Ding *et al* studied the growth of single and multilayer graphene on GaN/sapphire substrates with atmospheric pressure CVD at 950 °C and varying methane (CH_4) flows [31]. Later, Zhao *et al* [32] and Wang *et al* [33] evaluated the influence of the growth temperature and the carbon precursor on the quality of the directly grown graphene on GaN/sapphire substrates at 730 °C–1000 °C. All these approaches require relatively high growth temperatures, which can ultimately damage the GaN surface due to decomposition effects [34]. That's why Kim *et al* used a plasma-assisted CVD process to directly grow graphene on GaN-based LEDs at low temperatures (600 °C) [14]. Due to the diffusion of carbon atoms into the top *p*-GaN layer, they assumed that the directly grown graphene can form ohmic contacts. However, all of these direct growth processes were either performed at elevated temperatures and/or used hydrogen (H_2) as a process gas, both of which are known for inducing decomposition of the GaN surface [34–36].

Here, we report the direct growth of graphene on GaN in a single-step PECVD process under a GaN-protecting nitrogen (N_2) atmosphere at sample surface temperatures of <800 °C. By replacing the commonly used H_2 with N_2 as process gas, we were able to suppress GaN surface decomposition and enable the growth of graphene on both undoped and *p*-doped GaN substrates. We were able to increase the quality of the graphene by reducing the amount of CH_4 during growth. Adjusting the growth time allows for a trade-off between sheet resistance and transparency of the grown graphene layers. In a proof-of-concept experiment, we demonstrate both enhanced lateral current spreading and reduced operation voltage due to the directly-grown graphene CSL in GaN-based LEDs.

2. Experimental methods

Undoped (*u*-) GaN on sapphire and GaN-LEDs with a *p*-doped top layer were used as growth substrates during this study. The epitaxial GaN layers are grown in c-direction (0 0 0 1) in a wurtzite crystal structure. Prior to the growth process, the epi-wafers were scribed and cleaved into small samples (~1.5 × 1.5 cm^2) and subsequently cleaned with a standard cleaning process by dipping them into hot acetone, ethanol, isopropanol and dry blowing with N_2. The samples were then loaded into a 4-inch cold-wall PECVD system from AIXTRON Ltd (Black Magic Pro). The system is designed with a showerhead to support a homogeneous gas mixture in the reaction chamber. A top heater (located below the showerhead) and a bottom heater heat up the chamber to the desired growth temperature at a rate of 150 °C min^{-1}. The system temperature is directly measured with three separate thermocouples located at the bottom heater, the top heater and at the surface of the sample. Figure S1 (available online at stacks.iop.org/TDM/7/035019/mmedia) of the *supplementary information* shows the inside of the reactor chamber. The surface thermocouple is covered in a quartz sleeve and located directly on top of the substrate surface. If not otherwise stated, the temperatures mentioned in this work refer to the measured temperature at the bottom heater thermocouple. Hereby, bottom heater temperatures of 800 °C correlate with ~700 °C at the surface of the sample. Argon (Ar), N_2 and CH_4 were used for all processes. A typical process flow diagram is shown in figure S 2. During the heating phase, 250 sccm Ar and 1250 sccm N_2 were introduced into the system at a chamber pressure of 10 mbar. During the graphene growth phase (hereafter referred to as 'growth'), the Ar flow was shut down and a CH_4 flux of 5–15 sccm was adjusted with a constant N_2 flow of 200 sccm. The chamber pressure was maintained at 5 mbar throughout the growth. After the growth, the heaters were turned off and the samples cooled down at 10 mbar under an atmosphere of 500 sccm Ar and 500 sccm N_2.

Both heaters simultaneously act as electrodes to ignite a capacitively-coupled, pulsed DC plasma (rectangular pulse waveform) with pulse frequencies of up to 100 kHz provided by a TruPlasma DC40001 plasma generator. All processes in this work were done with a plasma power of 40 W and a pulse frequency of 10 kHz. More details about the pulsed DC

plasma and the plasma process are described elsewhere [37].

After the growth process, the samples were analyzed by scanning electron microscopy (SEM) and Raman spectroscopy. For Raman spectroscopy, we used a NTEGRA Spectra system from NT-MDT with a laser wavelength of 532 nm, a laser spot size of <0.5 μm and a spectral resolution of <4 cm^{-1}. A pinhole of $\sim$50 μm allows a surface-sensitive, confocal measurement to reduce background signals of the growth substrate. For optical transparency measurements, a UV–VIS Spectrophotometer from Shimadzu (UV-2550) was used. Transparencies of the samples were measured in a range of 350–750 nm. All transmission spectra were compared to bare *u*-GaN samples and GaN-LEDs with a *p*-doped top layer as a reference to obtain the transmission losses of the grown graphene. A four-point-probe station from SUSS MicroTec (PM5) was used for *I*-*V*-measurements and *transfer length* measurements (TLM). For TLM, the samples were prepared with 200 × 400 μm^2 Ti/Au contact pads with varying distances to determine the sheet resistance of the grown graphene layers. Additionally, conductive silver paint on the edge of the GaN-LED samples was applied as a *n*-contact. The plasma was analyzed by a 4-channel Avaspec-2048L-USB2-RM optical spectrometer system from AVANTES. The system has four spectrometers, which each work separately in a defined wavelength regime between 200 nm and 1000 nm. All spectrometers reach a resolution below 0.3 nm. The spectra were measured over a 4-channel optical fiber through a quartz window located at the outside of the reactor chamber. For comparability, all optical emission spectra were normalized to the sum of the integrated counts.

X-ray photoelectron spectroscopy (XPS) measurements were performed with a PHI Quantera II instrument using a monochromatic Al Kα source. All spectra were obtained at the take-off angles of 85°, 53°, 37° and 23.6° with a spatial resolution of $\sim$100 μm (at 45°). Charge compensation with a dual beam was performed during all measurements to neutralize possible surface charging effects due to electrons and Ar^+ ions.

3. Results and discussion

Figure 1(a) shows a SEM image of the surface of a *u*-GaN substrate after graphene deposition under N_2 atmosphere at a temperature of 800 °C. The GaN surface shows no indication of an increased decomposition process. This is important to enable the growth of graphene without destroying the GaN surface in our single-step PECVD process. Prior to our first growth attempts, we investigated the effect of high temperatures and different gas atmospheres (H_2 or N_2) to the GaN surface. Temperatures above 800 °C showed distinct surface decomposition effects after 1 h in the CVD system chamber under H_2 atmosphere (see figure S3). By using N_2 instead of H_2, we were able to suppress the surface decomposition for up to 1 h of growth time and temperatures above 850 °C. This shows the potential of N_2 to protect the surface of GaN substrates during our single-step PECVD process.

One of the most prominent ways to characterize the quality of graphene layers is Raman spectroscopy. Typical Raman features of pristine graphene comprise a G-peak ($\sim$1580 cm^{-1}) and a 2D-peak ($\sim$2680 cm^{-1}). The G-peak is the main signature for all *sp*^{2}-hybridized carbons and corresponds to the C-C bond stretching in the graphene lattice. It is associated with a symmetric phonon in the center of the Brillouin zone (**Γ**-point) [38]. The 2D-peak represents the breathing mode like stretching of C-C bonds in the graphene lattice and originates in a double-resonance process, involving a phonon at the **K**-point of the Brillouin zone. The 2D-peak holds information about the crystal structure and the number of stacked graphene layers [38]. In defective graphene sheets, other peaks can be observed in a Raman spectrum. The main features of defective graphene are the D-peak ($\sim$1350 cm^{-1}) and the D′-peak ($\sim$1620 cm^{-1}). Both peaks are due to disorder-induced scattering of phonons at defect sites in the lattice [38, 39] and are typically observed in nanocrystalline or highly damaged graphene [39–41].

Figure 1(b) shows the Raman spectra of graphene on *u*-GaN (dots) together with Lorentzian fits (solid lines) for growth times of 10 min (red), 30 min (blue) and 60 min (green) grown with 15 sccm of CH_4 and 200 sccm of N_2. After 10 min of growth, a distinctive Raman spectrum of defective graphene with a relatively high D-peak, a G-peak and a D′-peak is observable. At around $\sim$2690 cm^{-1} a small 2D-peak emerges. With increasing growth time, the intensity of the 2D-peak increases, while the intensity of the D-peak stays nearly constant. This indicates the growth of nanocrystalline graphene, where the D-peak results from the high amount of grain boundaries in the grown graphene layer [40]. The enhanced 2D-peak intensity is consistent with an increase in the long-range order of the crystal structure. However, due to the high density of defects (e.g. point defects), there is no reduction of the D-peak intensity observable. We were able to deposit nanocrystalline graphene on *u*-GaN for up to 60 min, while simultaneously protecting the GaN surface from decomposition due to temperature and plasma-induced etching effects. For comparison, the same growth process under H_2 atmosphere led to highly amorphous carbon layers and distinct damaging of the GaN surface (see figure S4).

It is known that a PECVD process has a higher dissociation of the carbon containing precursors compared to thermal CVD due to the physical component of collisions between free electrons, atoms and

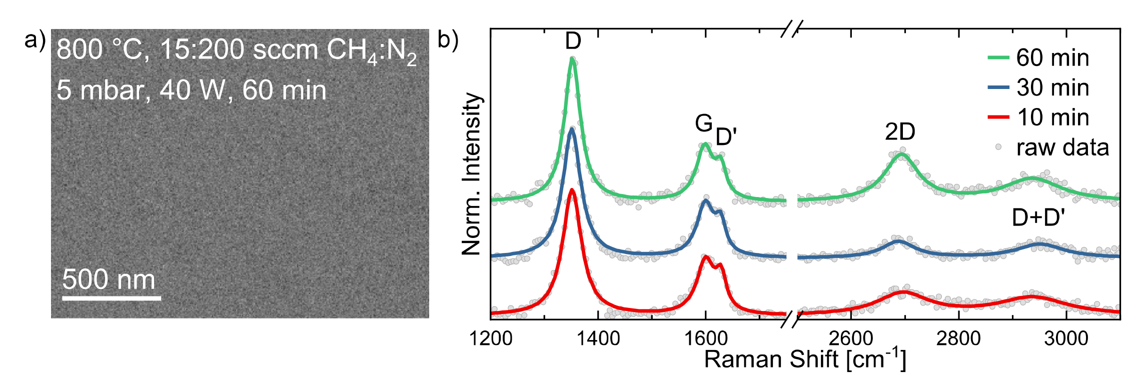

Figure 1. (a) SEM image of the *u*-GaN surface after 60 min of graphene growth at a temperature of 800 °C, a flux of 15 sccm: 200 sccm CH_4:N_2, a pressure of 5 mbar, and 40 W of plasma power. The image was taken under 1 kV acceleration voltage and detected by an In-Lens detector. (b) Corresponding Raman spectra of the grown graphene layers on *u*-GaN for 10 min (red), 30 min (blue) and 60 min (green) of growth time. All spectra were normalized to the G-peak and all peaks were fitted with single Lorentzian functions. The shaded dots show the original data as a reference after subtraction of the GaN-background.

molecules [42]. The higher dissociation can result in higher growth rates of graphene [14, 37]. Due to this plasma-enhanced dissociation, the growth rate can be adjusted by varying the concentration of the carbon containing source (e.g. CH_4) [31]. To investigate the influence of the CH_4 flux on the grown graphene, we increased (reduced) it to 30 sccm (5 sccm). Figure 2(a) shows the fitted Raman spectra of the graphene layer grown on the *p*-GaN surface of a fully operational LED sample with 5 sccm (green), 15 sccm (blue) and 30 sccm (red) of CH_4. For a flux of 30 sccm of CH_4, no distinctive Raman peaks originating from graphene can be observed in the grown layer. The D- and G-peak merge into a broad band and the 2D-peak is not observed anymore. Such a Raman spectrum is typical for highly amorphous, nanocrystalline carbon layers [43]. The long-range order of the lattice in such carbon layers is lost, which results in a broadening of the Raman peaks. Additionally, 30 sccm of CH_4 leads to a high GaN surface decomposition (see figure S5). The additional CH_4 in the 30 sccm CH_4 process (compared to the 15 sccm CH_4 process) is efficiently dissociated by the plasma. This leads to a high concentration of free hydrogen species in the chamber, which can chemically react with the nitrogen atoms at the GaN surface and result in a surface etching effect [34, 44]. To support this hypothesis, we conducted optical emission spectroscopy (OES) during the growth process for the various CH_4 fluxes (see figures S6(a)–(e) for the OES results). We see an increase in the intensity of the hydrogen related emission peaks (H_α, H_β and CH) with higher CH_4 amounts, indicating an increased dissociation of CH_4 molecules in the plasma.

When the CH_4 flux is reduced to 5 sccm, a distinctive Raman spectrum for graphene is obtained (see figure 2(a)). The defect-induced D- and D′-peaks are decreased when compared to the sample grown with 15 sccm CH_4. This change in the CH_4 flux also results in an increase in the 2D-peak. Figure 2(b) shows the intensity ratio between the 2D- and the G-peak (I_{2D}/I_G), the ratio between the D- and the G-peak (I_D/I_G) and the full width at half maximum (FWHM) of the G-peak. These peak intensity ratios are commonly used to gain information about the overall quality of the grown graphene. The I_D/I_G ratio decreases from ∼2.4 to ∼1.7 after a reduction of the CH_4 flux from 15 sccm to 5 sccm. This implies a decrease of the defect density of the grown graphene. Simultaneously, the I_{2D}/I_G ratio increases from ∼1 to ∼1.4. The FWHM of the 2D-peak decreases from ∼59 cm^{-1} to ∼45 cm^{-1} with decreasing amount of CH_4. This data indicates that the long-range order of the graphene crystal structure is increased with reduced CH_4 flux. To our knowledge, this is the best I_{2D}/I_G ratio for graphene directly grown on GaN-based substrates reported in literature. We attribute the increase of the graphene quality with lower CH_4 flows to a reduction in the concentration of active growth species at the *p*-GaN surface. This results in a decreased nucleation density when compared to the higher CH_4 flows. Therefore, the graphene grains can grow larger before they merge at their grain boundaries.

With this set of parameters (800 °C, 5 sccm: 200 sccm CH_4:N_2, 5 mbar, 40 W plasma power) we systematically increased the growth time from 0.5 to 1, 1.5, 2, 4 and 8 h to investigate a possible reduction in the defect density of the grown graphene. Figure 3(a) shows the fitted Raman spectra of the graphene layers grown on the *p*-GaN top layer of a GaN-LED for growth times of 0.5 h (bottom) and 4 h (top) (see figure S7 for the Raman spectra of all growth times). It is clearly shown that there is a decrease in intensity and a broadening of the D- and the 2D-peak with increasing growth time.

Figure 3(b), top, shows the I_D/I_G (black) and the I_{2D}/I_G (red) ratios versus growth time. Both the I_D/I_G and the I_{2D}/I_G ratios show a declining trend from a I_D/I_G (I_{2D}/I_G) ratio of ∼2 (∼1.2) for 0.5 h down

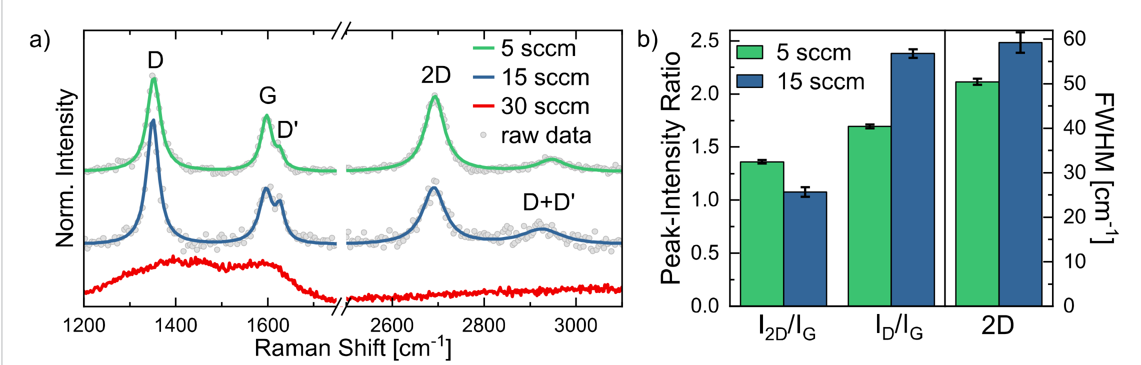

Figure 2. (a) Raman spectra of graphene grown at 5 sccm (green), 15 sccm (blue) and 30 sccm (red) of CH_4 on the *p*-GaN surface of a GaN-LED sample. The process parameters are the same as in figure 1 for the 60 min process. The spectra for 5 sccm and 15 sccm were normalized to the G-peak and all peaks were fitted with single Lorentzian functions. The shaded dots show the original data as a reference after subtraction of the GaN-background. (b) The left *y*-axis shows the peak-intensity ratio of the 2D- and G-peak and the D- and G-peak for 5 sccm (green) and 15 sccm (blue) of CH_4. The right *y*-axis shows the full width at half maximum (FWHM) of the 2D-peak for 5 sccm and 15 sccm of CH_4.

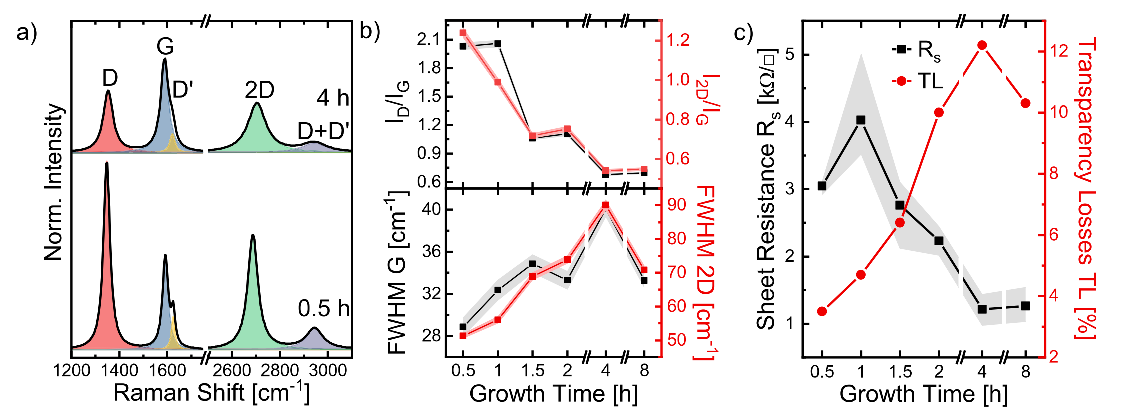

Figure 3. (a) Raman spectra of graphene layers for 0.5 h (bottom) and 4 h (top) growth time. The spectra were normalized to the G-peak and all peaks were fitted with single Lorentzian functions. (b) The I_D/I_G (top, black) and I_{2D}/I_G (top, red) ratios and the FWHM of the G (bottom, black) and 2D-peak (bottom, red) of the grown graphene layers for various growth times. The shaded areas represent the standard deviation of the fitting parameters. (c) The average sheet resistances R_s (black) and the corresponding average transparency losses TL in % (red) of the grown graphene layers for various growth times. The shaded areas represent the measurement errors.

to ~0.7 (~0.5) at 4 h of growth time. As the D-peak correlates with the defects in the graphene lattice, a decrease of the I_D/I_G ratio normally indicates a reduction of the defect density. At the same time the intensity of the 2D-peak should increase if the reduction of the I_D/I_G ratio solely stems from a lower defect density. Thus, the simultaneous decrease of I_{2D}/I_G and I_D/I_G cannot simply be described by the reduction of the defect density of our graphene layers. Additionally, we observe a red (blue) shift of the G-peak (2D-peak) of ~6 cm^{-1} (~16 cm^{-1}) and an increase of the integrated intensity of the G-peak by a factor of ~2 with increasing growth time (see figure S8). These trends are in good agreement with reports on the growth of multilayer graphene (MLG) [45–47]. Conclusively, we believe that increasing growth time leads to a growth of MLG in our process. Normally, the 2D-peak of MLG splits into multiple peaks, leading to a very distinctive broadening of the 2D-peak. A single Lorentzian function cannot be used for the fitting of such graphene layers [41]. However, this is only true for aligned MLG sheets with a certain orientation of each layer to each other. In case of turbostratic graphene, where no such fixed orientation is given, the 2D-peak shows no pronounced splitting effect and a single Lorentzian function can be used for fitting [46]. This indicates that our graphene layers have a turbostratic character. At the same time, we observe a non-neglectable broadening of the FWHM of both the G- (black) and the 2D-peak (red) with increasing growth time (see figure 3(b) bottom), which is consistent with the growth of multiple layers of graphene. SEM images of the graphene layers are shown in figure S 9 for various growth times. A change in the structure of the graphene layers can be observed with increasing growth time. At a growth time of 0.5 h, randomly ordered grains with an average diameter of ~100 nm cover the surface. With increasing growth time, the SEM contrast is decreasing, and a roughening of the

surface is found. We attribute this loss in contrast to the growth of turbostratic MLG, where randomly ordered graphene grains on top of each other lose their individual distinguishability. Following Cançado *et al* [43], we in addition estimate the average grain size and defect density from the Raman spectra of the graphene layers. Taking into account the FWHM of the D- and the G-peak, in addition to the increasing contribution of the D′-peak to the cumulative Raman spectrum, we can derive an average grain size of L_a ~30 nm and an average distance between defects of L_D ~2–5 nm for our samples.

To validate the assumption of the growth of MLG, we additionally conducted electro-optical measurements to extract the sheet resistance (R_s) and the transparency losses (TL) of our grown graphene layers. Figure 3(c) shows the average sheet resistance (black) and the average transparency losses (red) of the graphene layers for varying growth times. As the growth time increases, the average sheet resistance decreases from ~4 kΩ/□ (1 h) down to ~1.2 kΩ/□ (4 h). This reduction in sheet resistance is typical for MLG [48]. We calculated the average sheet resistance from various measurement points. The lowest measured sheet resistance was 1.02 kΩ/□ at 4 h of growth time. This value exceeds typical sheet resistances (~230 Ω/□) of high-quality, large-area CVD graphene grown on catalytic substrates (e.g. copper foil) [49], but is reduced compared to previously reported sheet resistances (~1.4 kΩ/□) of graphene directly grown on GaN via PECVD [14]. At the same time, the transparency losses of the graphene layers increase from ~3.5% (0.5 h) to ~12% (4 h), which is consistent with the growth of MLG. Compared to the absorption losses of monolayer graphene (~2.3%) we can estimate the growth of ~1–2 (0.5 h) up to ~5–6 (4 h) layers of graphene depending on the growth time. We want to emphasize that a possible doping of the graphene with nitrogen atoms could also lead to a change of the characteristic Raman ratios and the broadening of the peaks [50]. However, the trend of decreasing sheet resistance, the typical broadening of the Raman peaks and the higher absorption losses strongly support our assumption of the growth of MLG with increasing growth time.

XPS measurements were conducted to study the composition of the grown graphene layers. Figure 4(a) shows XPS spectra of a *u*-GaN reference (red) and the graphene/*u*-GaN samples for 1 h (blue) and for 4 h (green) of growth time. The *u*-GaN reference sample shows Ga related (Ga3s ~ 161 eV, Ga3p ~ 106 eV and Ga3d ~ 20 eV) and N related (N1s ~ 398 eV) peaks. A weak carbon related peak (~285.5 eV) can also be observed. With increasing growth time, the signals of the Ga and N related peaks decrease with a corresponding increase in the carbon related C1s peak. A good estimate for the increase of carbon species on the *u*-GaN surface can be found in the comparison between the C1s and the Ga related peaks with increasing growth time. The C1s/Ga3d ratio increases from ~0.3, for the reference, to ~0.9 (~2) for 1 h (4 h) of growth time. This proves that there is an increase in the amount of carbon on the *u*-GaN surface. To validate that the additional carbon on the surface corresponds to the growth of graphene layers, high resolution XPS spectra were measured, as can be seen in figure 4(b). The reference sample shows a relatively small peak at around 285.5 eV, which can be attributed to carbon contamination on the surface of the *u*-GaN surface. This value is in good agreement with C-OH/C-H [51] or sp^3-hybridized carbon species [52] reported in literature. For the 1 h and 4 h samples, the peak maximum is at 284.55 eV and 284.3 eV, respectively. These peaks can be attributed to the sp^2-hybridized C-C bonding of carbon atoms in the graphene lattice and are in excellent agreement with reported values for graphene layers in literature [40, 51, 53–55]. Also, the C1s peak of the 4 h sample shows a higher intensity compared to the 1 h sample. Thus, the XPS measurements substantiate the hypothesis of the growth of multilayer graphene with increasing growth time. There is a slight shift (~0.25 eV) of the C1s peak with increasing growth time observable. Due to the angle resolved, surface sensitive measurement, we attribute this shift to a decreasing contribution of the interaction between the first graphene layer and the substrate with increasing growth time. These different contributions (C-C vs. C-substrate) could result in slightly different binding energies. Also, we cannot conclusively exclude the influence of charging effects of the sample during the measurements or nitrogen doping of the graphene layers. Although such doping effects can in principle be detected by XPS measurements, we were not able to undoubtedly identify N-doping of the graphene layers because of the large background signals stemming from the GaN substrate.

Finally, we contacted the fully-operational GaN-LED with MLG grown on the *p*-doped side (growth time of 8 h) to analyze the current spreading effect of the grown graphene layers. This sample was chosen because it offered the best relation between transparency losses (~10%) and sheet resistance (~1.3 kΩ/□). Note, that this transparency loss is in accordance with requirements for transparent electrodes like ITO (typical transparency losses of ~10–20%). Additionally, the sheet resistance is far below the sheet resistance of typical p-GaN capping layers (≫30 kΩ/□). This makes our PECVD grown graphene highly attractive as transparent electrode in GaN-based LEDs. Ti/Au contacts from the TLM measurements were used as *p*-contact while conductive silver paint on the edge of the sample acted as the *n*-contact. Figure 5(a) depicts the *I*–*V* characteristics of a device with (blue) and a reference device without (red) a graphene CSL. Both devices show a typical rectifying behavior. The device with the graphene

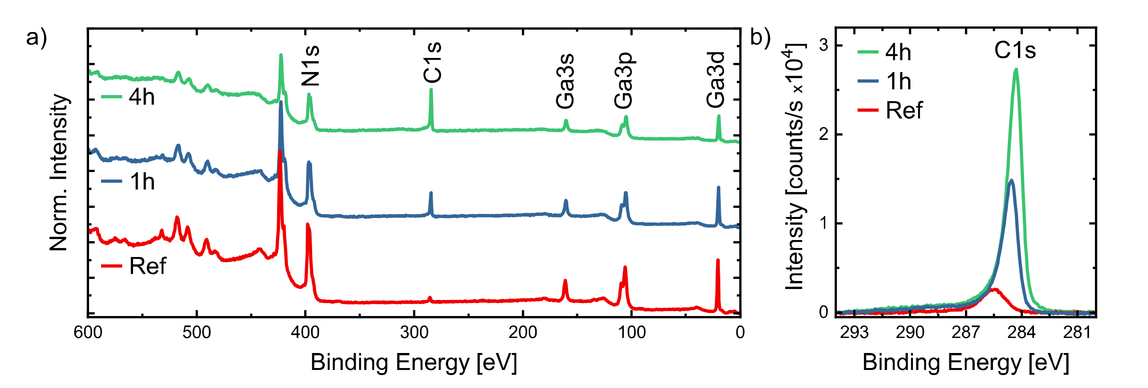

Figure 4. (a) XPS spectra of a *u*-GaN reference (red) and graphene/*u*-GaN samples for 1 h (blue) and 4 h (green) of growth time with a take-off angle of 85°. (b) The corresponding high resolution XPS spectra of the C-C related C1 s peak (∼284.5 eV) for 1 h and 4 h of growth time.

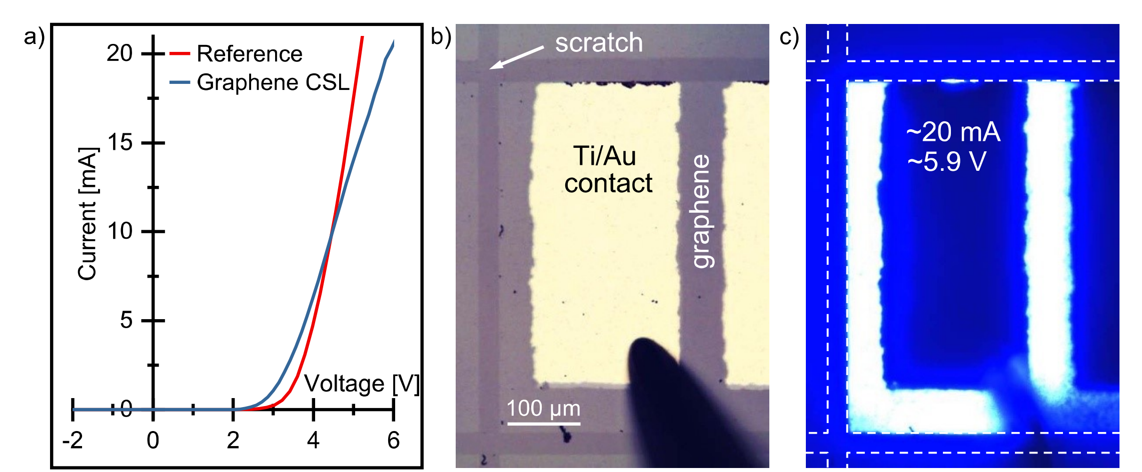

Figure 5. (a) *I-V*-measurements of a fully operational GaN-LED with graphene/*p*-GaN as top layer with (blue) and without graphene CSL (red). (b) shows the optical image of the corresponding GaN-LED surface with the graphene CSL. We scratched away the graphene around the Ti/Au metal contact to limit the current paths on the surface. (c) shows the light emission around the contact area of the biased GaN-LED with graphene CSL at 20 mA.

CSL shows a ∼0.6 V lower onset voltage of ∼3.2 V compared to the reference device (∼3.8 V). However, the *I*–*V* characteristic of the device with a graphene CSL has a slightly lower slope compared to the reference device. This can probably be attributed to resistance losses due to the processing of the contacts to the GaN-LED. Figure 5(b) presents an optical image of a 200 × 400 μm^2 Ti/Au pad as a *p*-contact on top of the MLG-CSL. The graphene was scratched away close to the contact structures to limit possible lateral current paths along the surface. Hereby, the light emission is limited by the area with the graphene CSL. Figure 5(c) shows an optical image of the biased LED at ∼20 mA. The blue light emission around the contact area demonstrates a distinct current spreading effect. Obviously, the scratched areas hinder the current path, leaving only the area with graphene illuminated. The clear proof of current spreading effect is attributed to the good ohmic contact between the graphene and the *p*-GaN layer on the one side combined with the low sheet resistance of the MLG on the other side. By measuring the illuminated area and subtracting the area of the Ti/Au contact, a comparison between the light emission of the device with graphene CSL and of the reference device can be drawn. When compared to the reference device (see figure S10), the graphene CSL device shows an ∼8 times larger emission area surrounding the contact area. This proves the potential of our directly grown graphene to work as a good transparent CSL for GaN-based LEDs.

4. Conclusion

In this work, graphene is successfully grown in a single-step PECVD growth process on GaN substrates and GaN-based LEDs by using a surface protecting N_2 atmosphere and growth temperatures below 800 °C. Compared to the commonly used H_2 atmosphere, the N_2 atmosphere shows less GaN surface decomposition while simultaneously enabling the growth of good quality graphene. By reducing the CH_4 flux

from 15 sccm to 5 sccm, the I_{2D}/I_G ratio increased from ∼1 to ∼1.4. This ratio exceeds the so far, best reported value for directly grown graphene on GaN in literature. Raman spectroscopy, TLM, XPS and transparency measurements show the growth of multilayer graphene (MLG) with increasing growth time of up to 8 h. The MLG shows a minimum sheet resistance of 1.02 kΩ/□ with transparency losses of up to ∼12%. The graphene works as current spreading layer with good ohmic contact and shows an ∼8 times increase in the emission area of GaN-LED while sustaining the rectifying behavior of the LED. This single-step PECVD process shows a potential pathway for further progress in the use of graphene as transparent conductors in GaN devices.

Acknowledgments

We thank Hans Lugauer and Adrian Avramescu from OSRAM Opto Semiconductors GmbH for their support during this work.

Jan Mischke acknowledges a scholarship from the International Max Planck Research School for Interface Controlled Materials for Energy Conversion (IMPRS-SurMat).

Joel Pennings acknowledges a research internship from the DAAD RISE Germany program with corresponding funding by Mitacs Canada.

ORCID iDs

Jan Mischke https://orcid.org/0000-0001-8384-8848
Joel Pennings https://orcid.org/0000-0002-8821-7225
Erik Weisenseel https://orcid.org/0000-0001-7279-4442
Michael Rohwerder https://orcid.org/0000-0002-2466-3963
Wolfgang Mertin https://orcid.org/0000-0001-6792-6033
Gerd Bacher https://orcid.org/0000-0001-8419-2158

References

[1] Lee H C, Liu W-W, Chai S-P, Mohamed A R, Lai C W, Khe C-S, Voon C H, Hashim U and Hidayah N M S 2016 *Procedia Chem.* **19** 916–21
[2] Li X *et al* 2009 *Science* **324** 1312–14
[3] Li X, Zhu Y, Cai W, Borysiak M, Han B, Chen D, Piner R D, Colombo L and Ruoff R S 2009 *Nano Lett.* **9** 4359–63
[4] Somani P R, Somani S P and Umeno M 2006 *Chem. Phys. Lett.* **430** 56–59
[5] Obraztsov A N, Obraztsova E A, Tyurnina A V and Zolotukhin A A 2007 *Carbon* **45** 2017–21
[6] Luo D *et al* 2019 *Adv. Mater.* **31** 1903615
[7] Lee H C, Liu W-W, Chai S-P, Mohamed A R, Aziz A, Khe C-S, Hidayah N M S and Hashim U 2017 *RSC Adv.* **7** 15644–93
[8] Sun J *et al* 2015 *Nano Res.* **8** 3496–504
[9] Zhang L, Shi Z, Wang Y, Yang R, Shi D and Zhang G 2011 *Nano Res.* **4** 315–21
[10] Wei D, Peng L, Li M, Mao H, Niu T, Han C, Chen W and Wee A T S 2015 *ACS Nano* **9** 164–71
[11] Kim Y S, Joo K, Jerng S-K, Lee J H, Yoon E and Chun S-H 2014 *Nanoscale* **6** 10100–5
[12] Wei D, Lu Y, Han C, Niu T, Chen W and Wee A T S 2013 *Angew. Chem. Int. Ed.* **52** 14121–6
[13] Malesevic A, Vitchev R, Schouteden K, Volodin A, Zhang L, van Tendeloo G, Vanhulsel A and van Haesendonck C 2008 *Nanotechnology* **19** 305604
[14] Kim Y S, Joo K, Jerng S-K, Lee J H, Moon D, Kim J, Yoon E and Chun S-H 2014 *ACS Nano* **8** 2230–6
[15] Xiong F, Guo W, Feng S, Li X, Du Z, Le Wang D J and Sun J 2019 *Materials* **12** 3533
[16] Li Z, Xu Y, Cao B, Qi L, Zhao E, Yang S, Wang C, Wang J, Zhang G and Xu K 2019 *AIP Adv.* **9** 095060
[17] Kneissl M, Seong T Y, Han J and Amano H 2019 *Nat. Photonics* **13** 233–44
[18] Bonaccorso F, Sun Z, Hasan T and Ferrari A C 2010 *Nat. Photonics* **4** 611–22
[19] Chen C H, Chang S J, Su Y K, Chi G C, Chi J Y, Chang C A, Sheu J K and Chen J F 2001 *IEEE Photonics Technol. Lett.* **13** 848–50
[20] Castro N A H, Guinea F, Peres N M R, Novoselov K S and Geim A K 2009 *Rev. Mod. Phys.* **81** 109–62
[21] Jo G *et al* 2010 *Nanotechnology* **21** 175201
[22] Hoon Seo T, Kyoung Kim B, Shin G, Lee C, Jong Kim M, Kim H and Suh E-K 2013 *Appl. Phys. Lett.* **103** 051105
[23] Li Z, Kang J, Liu Z, Du C, Lee X, Li X, Wang L, Yi X, Zhu H and Wang G 2013 *AIP Adv.* **3** 042134
[24] Kun X, Chen X, Jun D, Yanxu Z, Weiling G, Mingming M, Lei Z and Jie S 2013 *Appl. Phys. Lett.* **102** 162102
[25] Min Lee J, Yong Jeong H, Jin Choi K and Il Park W 2011 *Appl. Phys. Lett.* **99** 041115
[26] Joo K, Jerng S-K, Kim Y S, Kim B, Moon S, Moon D, Lee G-D, Song Y-K, Chun S-H and Yoon E 2012 *Nanotechnology* **23** 425302
[27] Zhang Y, Li X, Wang L, Yi X, Wu D, Zhu H and Wang G 2012 *Nanoscale* **4** 5852–5
[28] Chandramohan S *et al* 2013 *ACS Appl. Mater. Interfaces* **5** 958–64
[29] Chandramohan S, Ko K B, Han Yang J, Deul Ryu B, Katharria Y S, Yong Kim T, Jin Cho B and Hong C-H 2014 *J. Phys. D: Appl. Phys.* **115** 054503
[30] Sun J *et al* 2012 *IEEE Trans. Semicond. Manufact.* **25** 494–501
[31] Ding X, Sun H and Gu X 2014 *Chem. Vap. Deposition* **20** 125–9
[32] Zhao Y *et al* 2014 *Chinese Phys.* B **23** 096802
[33] Wang B, Zhao Y, Yi X-Y, Wang G-H, Liu Z-Q, Duan R-R, Huang P, Wang J-X and Li J-M 2016 *Front. Phys.* **11** 116803
[34] Mastro M A, Kryliouk O M, Anderson T J, Davydov A and Shapiro A 2005 *J. Cryst. Growth* **274** 38–46
[35] Rebey A, Boufaden T and El Jani B 1999 *J. Cryst. Growth* **203** 12–17
[36] Davydov A V and Anderson T J 1998 Thermodynamic analysis of the Ga-N system *III-V Nitride Materials and Processes III* ed T D Moustakas, S E Mohney and S J Pearton (Boston, MA: ECS), PV 98–18, p 38-49 https://www.ctcms.nist.gov/~davydov/98Davy_Ga-N_ECS_98_38.pdf
[37] Bekdüz B, Beckmann Y, Mischke J, Twellmann J, Mertin W and Bacher G 2018 *Nanotechnology* **29** 455603
[38] Jorio A 2012 *ISRN Nanotechnol.* **2012** 1–16
[39] Childres I, Jauregui L A, Park W, Caoa H and Chena Y P 2013 Raman spectroscopy of graphene and related materials new developments in photon and materials research vol 1, ed J I Jang (Hauppauge, New York: Nova Science Publishers Inc) https://www.scopus.com/record/display.uri?eid=2-s2.0-84895373577&origin=inward&txGid=1ce91176ac9e581a45e875288d2dddf1
[40] Oliveira M H, Schumann T, Gargallo-Caballero R, Fromm F, Seyller T, Ramsteiner M, Trampert A, Geelhaar L, Lopes J M and Riechert H 2013 *Carbon* **56** 339–50

[41] Ferrari A C 2007 *Solid State Commun.* **143** 47–57
[42] Hash D B and Meyyappan M 2003 *J. Phys. D: Appl. Phys.* **93** 750
[43] Cançado L G, Da Silva M G, Martins Ferreira E H, Hof F, Kampioti K, Huang K, Pénicaud A, Achete C A, Capaz R B and Jorio A 2017 *2D Mater.* **4** 025039
[44] Furtado M and Jacob G 1983 *J. Cryst. Growth* **64** 257–67
[45] Lenski D R and Fuhrer M S 2011 *J. Phys. D: Appl. Phys.* **110** 013720
[46] Garlow J A, Barrett L K, Wu L, Kisslinger K, Zhu Y and Pulecio J F 2016 *Sci. Rep.* **6** 19804
[47] Tay R Y, Park H J, Lin J, Ng Z K, Jing L, Li H, Zhu M, Tsang S H, Lee Z and Teo E h T 2018 *Chem. Mater.* **30** 6858–66
[48] Robinson J T, Culbertson J, Berg M and Ohta T 2018 *Sci. Rep.* **8** 2006
[49] Xu X *et al* 2017 *Sci. Bull.* **62** 1074–80
[50] Boas C R S V, Focassio B, Marinho E, Larrude D G, Salvadori M C, Leão C R and dos Santos D J 2019 *Sci. Rep.* **9** 13715
[51] Soin N, Ray S C, Sarma S, Mazumder D, Sharma S, Wang Y-F, Pong W-F, Roy S S and Strydom A M 2017 *J. Phys. Chem.* C **121** 14073–82
[52] Manojkumar P A, Krishna N G, Mangamma G and Albert S K 2019 *Phys. Chem. Chem. Phys.* **21** 10773–83
[53] Gao H *et al* 2012 *Carbon* **50** 4476–82
[54] Xiong B, Zhou Y, O'Hayre R and Shao Z 2013 *Appl. Surf. Sci.* **266** 433–9
[55] Wei N *et al* 2019 *ACS Nano* **13** 7517–26